JOURNAL OF GEOPHYSICAL RESEARCH, VOL. 95, NO. D8, PAGES 11,717-11,728, JULY 20, 1990

Discrete Angle Radiative Transfer
2. Renormalization Approach for Homogeneous and Fractal Clouds

PHILIP GABRIEL,[1] SHAUN LOVEJOY, ANTHONY DAVIS,[2]
DANIEL SCHERTZER[2] AND GEOFFREY L. AUSTIN

Physics Department, McGill University, Montréal, Québec, Canada

The discrete angle radiative transfer systems discussed in part 1 readily lend themselves to approximation schemes in which simple scaling systems with known radiative transfer properties can be doubled in size yielding analytic expressions relating the transfer coefficients corresponding to the initial and doubled scale. This "real space renormalization" method can be viewed as a generalization of conventional invariant imbedding techniques to scaling systems. Analytic nonlinear doubling mappings are obtained for homogeneous square, cubic and triangular systems, as well as for a simple fractal system with both open and cyclic horizontal boundary conditions. The doubling mappings have both thick and thin cloud fixed points; to which the transmission and albedoes are respectively algebraically attracted and repelled, with universal (phase function independent) exponents we estimate analytically. The method is approximate since it systematically neglects small-scale intensity gradients; however, the results are qualitatively correct, and it therefore establishes the connection between the scaling of the cloud optical density field and the scaling of the corresponding transfer coefficients. We also discuss the limitations of the method; in part 3 we compare it with a numerical approach.

1. INTRODUCTION

1.1. *Review*

In part 1 of this series [*Lovejoy et al.*, this issue], we propose the study of Discrete Angle (DA) radiative transfer systems which involve the coupling of only a small number of intensity fields. These systems are considerably simpler to deal with than the more usual (continuous angle, fully coupled) systems, yet are general enough to provide new insight into radiative transfer in inhomogeneous media. As in any system of partial differential equations, the DA equations can be given a number of discrete (lattice) approximations. In part 1, we obtained these directly from the interaction principle [*Preisendorfer*, 1965], a particularly simple discretization which involves a straightforward interpretation in terms of single-cell transfer coefficients, and provides the natural starting point for the method described here. We have

$$I_i(m) = \sum_k \sigma_{ik}(m)\, I_k[(m - k)] \qquad (1)$$

when no internal sources are present. $I_k(m)$ is the DA intensity in direction k (i.e., unit vectors along lattice directions) at position m in the lattice coordinate system, and

$$\sigma = \begin{pmatrix} T & R \\ R & T \end{pmatrix} \begin{pmatrix} T & R & S & S \\ R & T & S & S \\ S & S & T & R \\ S & S & R & T \end{pmatrix} \begin{pmatrix} T & R & S & S & S & S \\ R & T & S & S & S & S \\ S & S & T & R & S & S \\ S & S & R & T & S & S \\ S & S & S & S & T & R \\ S & S & S & S & R & T \end{pmatrix} \qquad (2)$$

for DA(d, $2d$) systems with $d = 1, 2, 3$ (see part 1 for the notation). In this case the lattice coordinate system is assumed to be orthogonal and single-cell "scattering" occurs in angles of 0, $\pi/2$, π with transfer coefficients T, S, R respectively, i.e., $T+R+2(d-1)S+A = 1$, where A is the absorption coefficient. In this paper, we are particularly interested in conservative ($A = 0$) systems where cells are either full (and identical in terms of σ) or empty, in which case $\sigma = 1$ (the unit matrix).

We then showed how to obtain the DA radiative transfer equations in the limit of the lattice size going to zero by ensuring that the the absolute eigenvalues of the transfer matrix σ approached the value one, i.e., either $T \to 1$, $R \to 0$ or $R \to 1$, $T \to 0$. It was noted that in conservative scattering, the DA systems involve four basic regimes determined by $\infty > pq > 0$, $pq = 0$ or $-\infty < pq < 0$, or $|pq| = \infty$ where q and p are related to the first and second Legendre coefficients of the (DA) phase function, respectively; see section 4 of part 1. The first, physically relevant regime is obtained by the limit $T \to 1$, $R \to 0$ with $S > 0$, the second is an uninteresting one-dimensional diffusion regime obtained in the same limit but with $S = 0$, and the third obtained in the limit $R \to 1$, $T \to 0$ is an unphysical regime characterized by negatively valued DA phase functions and the fourth, obtained for example with T=R=S is a discretized diffusion equation.

We then stated without too much justification that in scaling systems with conservative scattering we expect the following behavior as the optical thickness (τ) becomes very large:

$$T - T^* \approx h_T(\mathbf{P})\, \tau^{-\nu_T}$$
$$R^* - R \approx h_R(\mathbf{P})\, \tau^{-\nu_R} \qquad (3)$$

where $\mathbf{P}$ is a matrix with the same symmetry as σ in (2) describing the DA phase function. As a result of exact DA similarity relationships, we showed in scaling systems that the exponents ν_T and ν_R were universal (i.e., $\mathbf{P}$ independent). In contrast to this, the prefactors h_T and h_R are expected to depend on $\mathbf{P}$, according to general formulas discussed in part 1.

1.2. *Nonlinear Maps and Real Space Renormalization in DA Systems*

Below, we justify the scaling relations (3) for a number of

[1] Now at CIRA, Dept. of Atmospheric Science, Colorado State University, Fort Collins.

[2] Now at Établissement d'Études et de Recherches Météorologiques, Centre de Recherches en Météorologie Dynamique, Paris, France.

Paper number 89JD03147.
0148-0227/90/89JD-03147$05.00

systems, making use of a renormalization group approach which allows us to estimate the relevant exponents both analytically and numerically. Renormalization is very similar to the concept of invariant imbedding [*Bellman et al.*, 1960] which has been widely applied to (continuous angle) radiative transfer through plane-parallel media both semi-infinite [*Ambarzumian*, 1942] and finite [*Chandrasekhar*, 1950] under the generic name of "adding" (in this case, an infinitesimal layer to the given medium and applying principles of invariance). The closely related idea of "doubling" (of a given layer) has been used as an computationally efficient alternative to standard methods of solving the plane-parallel radiative transfer problem [*Hansen*, 1969] by starting with a very thin layer well described by single scattering in closed form. This computational method has recently been extended to horizontally finite homogeneous [*Cogley*, 1981] and internally inhomogeneous horizontally periodic media [*Stephens*, 1986]; our approach is more analytical.

Essentially, renormalization as applied here aims to estimate the global R and T coefficients of an optically thick system by repeatedly doubling the size of the system (or more generally quadrupling, etc.) starting with (optically thin) single cell transfer coefficients. Specifically, we obtain approximate doubling relations expressing the transfer matrix $\sigma(2\tau)$ in terms of $\sigma(\tau)$, i.e., $\sigma(2\tau) = f[\sigma(\tau)]$, where f is a nonlinear function to be evaluated for specific cloud geometries and we associate a σ matrix with the global response of the medium. Thus we have transformed a relatively complex boundary value problem for a linear system of partial differential equations into an approximately equivalent nonlinear algebraic one. As we shall see, although (for reasons detailed in section 4) the method is not very accurate quantitatively, it is qualitatively correct and provides insight into the basic transfer processes, especially in the optically thin and thick limits (the latter are explored numerically by *Davis et al.* [1989] and in part 3 [*Davis et al.*, this issue]).

The optical properties of very thick clouds can then be obtained by iteration: $\sigma(2^n\tau) = f^{(n)}[\sigma(\tau)]$ where we have used the notation $f^{(n)}$ for the n^{th} iterate of f. The properties of $f^{(n)}$ such as fixed points and scaling exponents can then be studied using functional iteration methods [e.g., *Schuster*, 1989]. As the thickness of the cloud is doubled, the albedo approaches 1 and near the fixed point, $R = 1$, $T = 0$, the iteration is approximated by matrix multiplication, yielding a power law (scaling) behavior governing the approach of R to 1 and T to 0. Recalling that the latter coefficients correspond to $pq < 0$, we may already anticipate that the exponents will be generally not be the same as those with $pq > 0$. Nevertheless, although at best the method is approximate, it gives insight into the thick and thin cloud limits and shows how thick cloud DA phase function independent exponents arise, as well as the converse (phase function sensitivity) which arises in the thin cloud limit. It also shows why we expect the albedo and transmission to scale when the medium itself is scaling. This formulation also has the advantage of being at once analytical and applicable to certain fractal clouds as we shall see in section 3.

The method described below is actually a type of "real space" renormalization, a method used to study the large scale behavior of many nonlinear physical systems (perhaps the simplest being the percolation problem mentioned in part 1). More precise (and more theoretically satisfying) renormalization approaches operate in Fourier-space, but these are outside our scope. Although the material presented in this paper is fairly self-contained it is primarily motivated by the desire to understand radiative transfer in inhomogeneous systems discussed in part 1, and its numerical predictions will primarily be discussed in part 3.

To the best of our knowledge, there is only one other instance in the literature of explicit application of renormalization methods to radiative transfer: spectral line transfer with complete frequency redistribution (incoherent isotropic scattering), a subject of interest in the theory of stellar atmospheres. *Bell et al.* [1978] retrieve known scaling results by a (Fourier space) renormalization procedure. In this problem, photons with different frequencies have different path distributions: "core" photons diffuse through the (slightly absorbing) medium, whereas "wing" photons exhibit strongly nonlocal behavior. This recalls ordinary (coherent) multiple scattering of photons through a medium with dense and tenuous regions, which in broad terms, is exactly the effect we attempt to model here.

It is interesting to note that in one spatial dimension the symmetries are such that the spatially discretized DA(1, 2) system can be solved exactly using very simple functional analysis applied to "adding" relations in the case of conservative scattering; see Appendix A. Of course, this exercise yields once again the plane-parallel result $\nu_T = \nu_R = 1$. The case of nonconservative scattering the DA(1, 2) system is also solvable exactly via renormalization (i.e. "doubling"), see Appendix C.

2. Asymptotic Scaling Properties of Horizontally Finite Homogeneous Clouds: Analytical Estimates

2.1. *Doubling Cubic, Square, and Triangular Media*

We illustrate the doubling method in detail with $d = 2$ by calculating the radiative transfer properties of the 2 x 2 square made up of square cells with $S(\tau)$, $T(\tau)$, $R(\tau)$ coefficients as defined in (2) and illustrated in Figure 1*a*. Appendix B gives the full details in the square lattice case with particular attention to the necessary approximations. We irradiate the square with unit radiation incident on the top face only (i.e., the boundary conditions are $I_{-y}(x,2\tau)=1$, $I_{+y}(x,0)=0$ for $0\le x\le 2\tau$, and $I_{-x}(2\tau,y)=0$, $I_{+x}(0,y)=0$ for $0\le y\le 2\tau$). Applying (1) to the 2 x 2 square lattice system, ignoring gradients along individual cell faces (the approximation) and interpreting the total $+y$ intensity at the top as $R(2\tau)$, the total $-y$ intensity at the bottom as $T(2\tau)$, and that from the sides as $S(2\tau)$, we obtain

$$T(2\tau) = \frac{[T(\tau)+\Gamma_d(\tau)]^2}{1-[R(\tau)+\Gamma_d(\tau)]^2}$$
$$R(2\tau) = [R(\tau)+\Gamma_d(\tau)]\,[1+T(2\tau)] \tag{4}$$

where the index d refers to the (integer) dimension (=2 here) and

$$\Gamma_2(\tau) = \frac{S(\tau)^2}{1-R(\tau)} \tag{5}$$

Analogous calculations in $d = 1, 3$ (cube) give formulas identical to (4) except that $\Gamma_1(\tau) = 0$ and

$$\Gamma_3(\tau) = \frac{2S(\tau)^2}{1-R(\tau)-S(\tau)} \tag{6}$$

When there is absorption, the expression for $S(2\tau)$ is very complicated. However, in the case of conservative scattering, we have $S(2\tau) = [1-T(2\tau)-R(2\tau)]/2$. *Cogley* [1981] obtained partial results in this direction by formulating a three step procedure of doubling in each spatial dimension separately; he

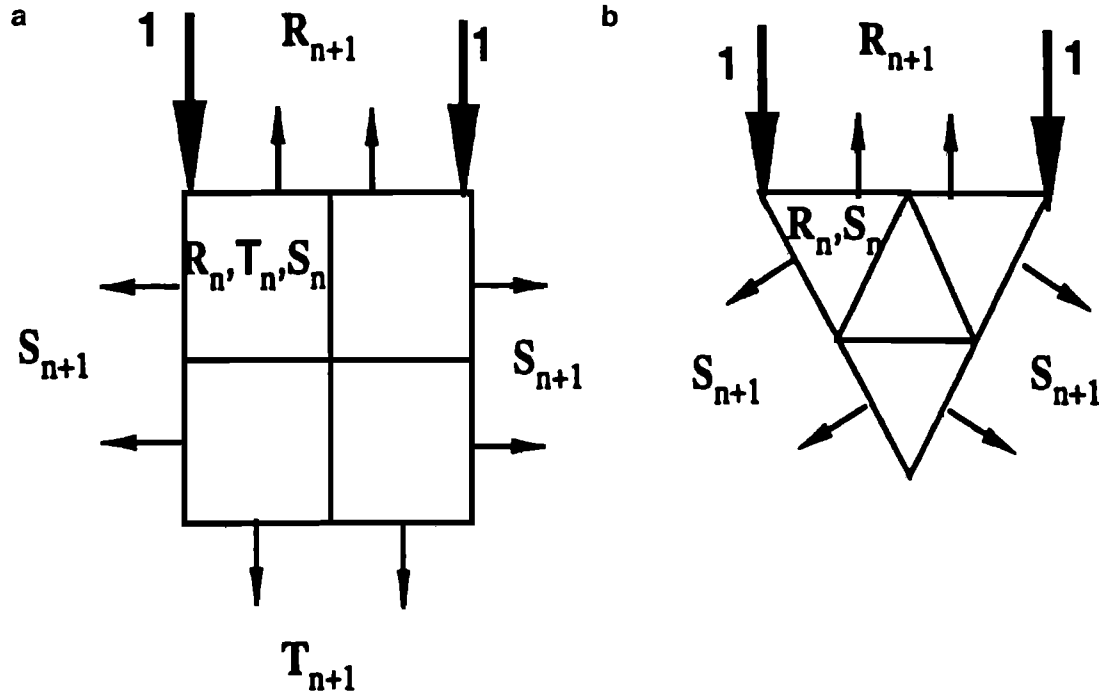

Fig. 1. Illustration of the doubling principle applied to (*a*) square and (*b*) triangular media. The averaged transfer coefficients in the nth iteration can be used as shown to calculate those in the $(n+1)$th iteration. Note that in the triangular case light can be only reflected or side-scattered, not transmitted directly.

then exploited his results numerically. Similarly, doubling triangles as shown in Figure 1*b* leads to

$$R(2\tau) = R(\tau) + \frac{2S(\tau)\Gamma_t(\tau)}{1-[R(\tau)+\Gamma_t(\tau)]^2+\Gamma_t(\tau)^2} \tag{7}$$

$$S(2\tau) = \backslash f(S(\tau),2)\ (1+S(\tau)^2+[S(\tau)+\Gamma_t(\tau)]^2) - \left(\frac{R(\tau)+\Gamma_t(\tau)}{1-[R(\tau)+\Gamma_t(\tau)]^2+\Gamma_t(\tau)}\right)^2 \tag{8}$$

where

$$\Gamma_t(\tau) = \frac{1}{2}[1-R(\tau)^2]\ [R(\tau)+S(\tau)]+R(\tau)S(\tau)^2 \tag{9}$$

In conservative scattering, $R+2S = 1$; hence R can be eliminated, leading to

$$S(2\tau) = \frac{S(\tau)}{2}\left(\frac{8 - 9S(\tau)}{5 - 6S(\tau)}\right) \tag{10}$$

2.2. *Fixed Points and Scaling Exponents*

The system of nonlinear equations (4) and (5) can now be regarded as a mapping $(T(2\tau), R(2\tau), S(2\tau)) = \mathbf{f}(T(\tau), R(\tau), S(\tau))$ and the functional behavior of $(T(\tau), R(\tau), S(\tau))$ over the whole range of τ can be analyzed by iterating to obtain

$$(T_n, R_n, S_n) = \mathbf{f}^{(n)}(T_0, R_0, S_0) \tag{11}$$

where we have used the notation $(T(2^n\tau_0), R(2^n\tau_0), S(2^n\tau_0)) = (T_n, R_n, S_n)$. In analyzing a nonlinear mapping such as (11), we must first determine its fixed points, i.e., those points which satisfy

$$(T^*, R^*, S^*) = \mathbf{f}(T^*, R^*, S^*) \tag{12}$$

where the asterisk indicates a fixed point value. Fixed points are either attractive or repulsive, depending on whether the mapping results in points in the infinitesimal neighborhood decreasing or increasing their distance from the fixed point. Mathematically, we require that the largest eigenvalue (Λ) of the Jacobian of **f** (evaluated at the fixed point), denoted

$$\mathbf{J} = \frac{\partial \mathbf{f}(T,R,S)}{\partial(T,R,S)}\Big|_{T^*,R^*,S^*} \tag{13}$$

is less than or greater than unity (the Jacobians will be explicitly evaluated in the following sections). Concentrating on the case of conservative scattering, we have

$$\mathbf{J} = \frac{\partial \mathbf{f}(T,R)}{\partial(T,R)}\Big|_{T^*,R^*} = \begin{pmatrix} \frac{\partial T_{n+1}}{\partial T_n} & \frac{\partial T_{n+1}}{\partial R_n} \\ \frac{\partial R_{n+1}}{\partial T_n} & \frac{\partial R_{n+1}}{\partial R_n} \end{pmatrix}_{T^*,R^*} \tag{14}$$

For reference, the derivatives when written out in full are as follows (for all three DA(d, $2d$) models)

$$\frac{\partial T_{n+1}}{\partial T_n} = 2T_{n+1}\left(\frac{1}{T_n+\Gamma_n}\left(1+\frac{\partial \Gamma_n}{\partial R_n}\right) + \frac{R_n+\Gamma_n}{1-(R_n+\Gamma_n)^2}\frac{\partial \Gamma_n}{\partial T_n}\right) \tag{15a}$$

$$\frac{\partial T_{n+1}}{\partial R_n} = 2T_{n+1}\left(\frac{R_n+\Gamma_n}{1-(R_n+\Gamma_n)^2}\left(1+\frac{\partial \Gamma_n}{\partial R_n}\right) + \frac{1}{T_n+\Gamma_n}\frac{\partial \Gamma_n}{\partial T_n}\right) \tag{15b}$$

$$\frac{\partial R_{n+1}}{\partial T_n} = (R_n+\Gamma_n)\frac{\partial T_{n+1}}{\partial T_n} + (1+T_{n+1})\frac{\partial \Gamma_n}{\partial T_n} \tag{15c}$$

$$\frac{\partial R_{n+1}}{\partial R_n} = (R_n+\Gamma_n)\frac{\partial T_{n+1}}{\partial R_n} + (1+T_{n+1})\frac{\partial \Gamma_n}{\partial R_n} \tag{15d}$$

where Γ_n will of course depend on d. For instance, in $d = 2$, Γ_n is obtained from (5) with $S_n = (1-T_n-R_n)/2$, i.e.,

$$\Gamma_n = \frac{1}{4}\left(\frac{T_n^2}{1-R_n} + 1-R_n - 2T_n\right) \tag{16a}$$

hence

$$\frac{\partial\Gamma_n}{\partial T_n} = \frac{1}{2}\left(\frac{T_n}{1-R_n} - 1\right) \tag{16b}$$

$$\frac{\partial\Gamma_n}{\partial R_n} = \frac{1}{4}\left(\left(\frac{T_n}{1-R_n}\right)^2 - 1\right) \tag{16c}$$

Continuing our study of the $d = 2$, conservative scattering case, we may drop explicit reference to S, and consider only the points in (T,R) space. Using **f** defined by (4) and (5), and imposing the condition (12), we obtain the following fixed points

(0,1)	stable	thick cloud
(1,0)	unstable	thin cloud
(1/2,-1/2)	unstable	unphysical
(-1/9,∞)	unstable	unphysical

Similarly, for the cubic lattice, we obtain

(0,1)	stable	thick cloud
(1,0)	unstable	thin cloud
(1/3,-2/3)	unstable	unphysical
(-1/25,∞)	unstable	unphysical

whereas for the triangular lattice, setting $S(2\tau) = S(\tau) = S^*$ in (10) yields $S^* = 0, 2/3$.

Since R and T must be positive and such that $R+T \le 1$, physically realizable points (T, R) must lie in the "physical triangle" defined by the points (0,0), (1,0), (0,1). Figures 2*a* and 2*b* show the results of iterating (4) for points starting very near the unstable thin cloud fixed point (1,0), for $d = 2, 3$ respectively.

We now seek to study the behavior of **f** near the fixed points by expanding **f** in a Taylor series (to first order only). Define

$$X_n = \begin{pmatrix} \Delta T_n \\ \Delta R_n \end{pmatrix} = \begin{pmatrix} T_n - T^* \\ R_n - R^* \end{pmatrix} \tag{17}$$

As long as the Jacobian is nondegenerate (see Appendix C for the degenerate case that arises in nonconservative scattering), near the fixed point we have $X_n = \mathbf{J}X_{n-1}$ or $X_n = \mathbf{J}^n X_0$ where $X_0 = (\Delta T_0, \Delta R_0)^T \approx (0,1)^T$ (see section 2.3); the superscript "T" designates matrix transposition. If we now write $\mathbf{J} = \mathbf{M}^{-1}\Lambda\mathbf{M}$, where Λ is a diagonal matrix (and **M** is a diagonalizing matrix) then

$$X_n = \mathbf{M}^{-1}\Lambda^n\mathbf{M}X_0 = \mathbf{M}^{-1}\begin{pmatrix} \Lambda_1^n & 0 \\ 0 & \Lambda_2^n \end{pmatrix}\mathbf{M}X_0 \tag{18}$$

and for large n (near the fixed point), X_n is dominated by the largest eigenvalue of **J**, denoted by $\Lambda = \max(\Lambda_1, \Lambda_2)$. Thus $\Delta T_n = \Delta T(2^n\tau) \approx \Lambda^n \Delta T_0$, and similarly for ΔR_n. Hence, we arrive at the following expressions:

$$\Delta T(\tau) = h_{T2}\,\tau^{-\nu_2}$$
$$\Delta R(\tau) = h_{R2}\,\tau^{-\nu_2} \tag{19}$$

with $\nu_2 = -\log(\Lambda)/\log(2)$, whereas h_{T2} and h_{R2} are determined by the matrix **M**; the subscript "2" indicates "doubling".

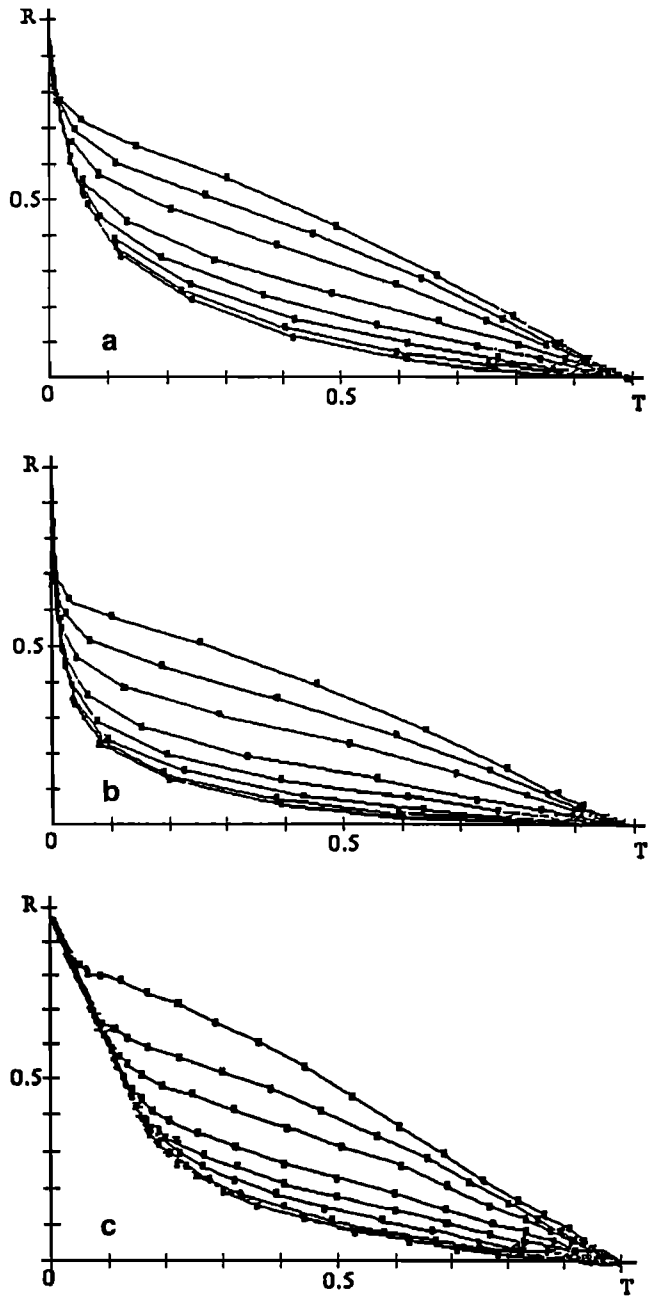

Fig. 2. (R,T) plot obtained by doubling method for (*a*) $d = 2$ using (4) and (5) iteratively. The curves top to bottom are for doubling of λ (the size parameter, proportional to τ) starting with $T = 0.99$ and $S/R = 0.1$, 0.2, 0.5, 1.0, 2.0, 5.0, 10, and 20, respectively. Note that as the curves approach the thick cloud fixed point (0,1), the absolute slope (w) becomes constant ($w \to w^* = 13.93\cdots$) as expected. Each point represents successive iterations; near the (0,1), they converge algebraically fast, the corresponding exponent is $\nu_2 = 0.447\cdots$ as discussed in the text. (*b*) For $d = 3$ with (6), the slope and scaling exponent near (0,1) are $w^* = 42.26\cdots$ and $\nu_2 = 0.28\cdots$, respectively. (*c*) For the $D = 1.58\cdots$ fractal; $w^* = 3.266$ and $\nu_2 = 0.147$.

2.3. *Thin Cloud Limit: Sensitive Dependence on the Phase Function and Extent of the Linear Regime*

Any approach to radiative transfer must clearly distinguish the thin and thick cloud limits. Our renormalization approach does this in a natural way by associating the thin cloud limit with an unstable, repelling fixed point (and hence sensitive dependence

on initial conditions, such as phase functions), and the thick cloud limit with stable, attracting fixed points and with universal behavior (lack of phase function sensitivity). Here we examine in more detail the properties of thin clouds, using the mapping (4) and (5). As outlined in section 3.2 of part 1, we may expect that near the thin cloud fixed point, that the transfer coefficients T,R,S depend linearly on τ. Furthermore, the linear regime is expected to extend to greater or smaller values of τ depending on the value $1-g$ where $g=t-r$ is the asymmetry factor characterizing the extent of forward (conservative) scattering (Appendix D in part 1); we have reintroduced the DA phase function matrix P_{ij} with elements $t=P_{\pm i\pm i}$, $r=P_{\pm i\ \mp i}$ and $s=P_{\pm i\pm j}=P_{\pm i\ \mp j}$ for $i\neq j$ (see subsection 3.3 in part 1).

In this subsection, we show how these results are determined by the properties of the neighbourhood of the thin cloud fixed point and derive these results from the mapping **f**. The thin cloud fixed point is $(T^*,R^*)=(1,0)$. Inserting these values into the Jacobian using the equations following (16) yields

$$\frac{\partial \mathbf{f}(T,R)}{\partial(T,R)}\Big|_{T^*,R^*} = \begin{pmatrix} 2 & 0 \\ 0 & 2 \end{pmatrix} \tag{20}$$

or, $\Lambda_1=\Lambda_2=2=\Lambda$; $\nu_2=-1$. Thus, for small τ we obtain (recalling that $\tau_n=2^n\tau_0$) the relationship

$$\begin{pmatrix} 1-T \\ R \end{pmatrix} = \tau_n \begin{pmatrix} 1-T_0 \\ R_0 \end{pmatrix} \tag{21}$$

This result is simply the familiar linearity relation for thin clouds. A direct consequence of (21) is that the properties of two thin clouds, identical except for the precise values of their discrete angle phase functions, will have linearly diverging albedoes and transmittances. In other words, error in our initial assumptions will be amplified. In the language of nonlinear dynamics, the optical properties of thick clouds are "sensitively dependent" on the DA phase functions.

We may now estimate the limits to the linear regime by expanding $\mathbf{f}(T,R)$ to second order, and considering the second order term as a perturbation. We obtain

$$\begin{pmatrix} \Delta T_n \\ \Delta R_n \end{pmatrix} = 2\left[1 + \frac{1}{4}\Delta R_n \begin{pmatrix} 3\beta+1 & \beta+3 \\ \beta+3 & 3\beta+1 \end{pmatrix}\right] \begin{pmatrix} \Delta T_{n-1} \\ \Delta R_{n-1} \end{pmatrix} \tag{22}$$

where $\beta = \Delta T_0/\Delta R_0$. From first-order scattering, $\Delta R_n=r\tau_n$ and $\Delta T_n=(1-t)\tau_n$, we obtain $\beta = (1-t)/r$. The largest eigenvalue (Λ) is found to be

$$\Lambda = 2+2(\beta+1)\Delta R_n \tag{23}$$

The linear regime only holds for $\Lambda\approx 2$; hence we therefore require

$$\Delta R_n \ll \frac{1}{\beta+1} \tag{24}$$

or, using $g=t-r$,

$$(1-g)\tau_n \ll 1 \tag{25}$$

We see that, as expected from standard continuous angle theory, it is the value of $(1-g)\tau$ with respect to 1 that controls the importance of the nonlinearities; $(1-g)\tau$ may be viewed as the equivalent isotropic scattering optical thickness.

2.4. *Thick Cloud Limit: Scaling Exponents and Universality With Respect to DA Phase Functions*

The analysis of thick cloud behavior ($\tau\to\infty$) is more involved, since the Jacobian $\partial\mathbf{f}(T,R)/\partial(T,R)|_{0,1}$ depends on the direction in (T,R) space that the fixed point (0,1) is approached. More specifically, the various derivatives $\partial T_{n+1}/\partial T_n$, $\partial T_{n+1}/\partial R_n$, $\partial R_{n+1}/\partial T_n$, $\partial R_{n+1}/\partial R_n$ evaluated at the fixed point $T^*=0$, $R^*=1$ are indeterminate; to get a well-defined value, we must specify the direction in R-T space in which the fixed point is approached. This direction is most easily defined by the (negative) direction tangent $w = (1-R)/T$. The following calculation is required in order to find the limiting value of w. Eliminating R in favour of w in the mapping **f**, we obtain the new mapping:

$$\mathbf{g}: (T_n,w_n) \to (T_{n+1},w_{n+1}) \tag{26}$$

For $d = 2$ we find

$$T_{n+1} = \frac{(w_n+1)^3}{(3w_n-1)[8w_n/T_n - (3w_n-1)(w_n+1)]} \tag{27a}$$

$$w_{n+1} = -\frac{2T_n w_n(3w_n-1)}{w_n+1} + 2\left[\frac{3w_n-1}{w_n+1}\right]^2 - 1 \tag{27b}$$

Since we are interested in the behavior in the vicinity of (0,1), we set $T_{n+1}=T_n=T^*=0$ and seek solutions of (27b) satisfying $w_{n+1}=w_n=w^*$:

$$(w^* - 1)(w^{*2} - 14w^* + 1) = 0 \tag{28}$$

which yields

$$w^* = 1,\ 7\pm 4\sqrt{3} \tag{29}$$

By analyzing the (new) Jacobian $\partial\mathbf{g}(T,w)/\partial(T,w)|_{T^*,w^*}$ for the various fixed points, we find that the only stable (attracting) fixed point is $(T^*,w^*)=(0,7+4\sqrt{3})$. This means that under doubling, the ratio $(1-R)/T$ takes on a nontrivial limiting value $(7+4\sqrt{3}=13.93\cdots)$ as $\tau\to\infty$ which is phase function independent (i.e., independent of r,t,s). This phase function independence assures us that the approach to the fixed point (T^*,R^*) will also be phase function independent (universal). We now use this result to obtain the behavior of **f** in the vicinity of (0,1), by calculating the Jacobian $\mathbf{J}=\partial\mathbf{f}(T,R)/\partial(T,R)|_{T^*,R^*}$ in the limit $T\to 0$ and $w\to w^*=7+4\sqrt{3}$. Using the replacement $R=1-Tw$, and taking the indicated limits, the various elements of the Jacobian are

$$\frac{\partial T_{n+1}}{\partial T_n} = \frac{(w^*+1)^2}{2w^*(3w^*-1)}\left(1 + \frac{1-w^*}{2(2w^*-1)}\right)$$

$$\frac{\partial T_{n+1}}{\partial R_n} = \frac{(w^*+1)^2}{4w^{*2}}\left(\frac{1-w^*}{3w^*-1} + \frac{1+3w^{*2}}{2(3w^{*2}-1)}\right) \tag{30}$$

$$\frac{\partial R_{n+1}}{\partial T_n} = \frac{(w^*+1)^2}{2w^*(3w^*-1)}\left(1+\frac{1-w^*}{2(3w^*-1)}\right) + \frac{1-w^*}{2w^*}$$

$$\frac{\partial R_{n+1}}{\partial R_n} = \frac{(w^*+1)^2(1-w^*)}{4w^{*2}(3w^*-1)} + \frac{(w^*+1)^2(1+3w^{*2})}{8w^{*2}(3w^{*2}-1)} + \frac{1+3w^{*2}}{2w^*}$$

yielding for the largest eigenvalue of **J**, which can always be written

$$\Lambda = \frac{\mathrm{Tr}\,J}{2} + \sqrt{\left(\frac{\mathrm{Tr}\,J}{2}\right)^2 - \det J} \tag{31}$$

where we have here

$$\mathrm{Tr}\,J = \frac{61w^{*4}-16w^{*3}+3w^{*2}-8w^{*}-3}{8w^{*2}(3w^{*}-1)^2} \tag{32a}$$

$$\det J = \frac{(w^{*}+1)^3}{4w^{*}(3w^{*}-1)} \tag{32b}$$

Inserting the value $w^{*}=7+4\sqrt{3}$, we obtain

$$\Lambda = \sqrt{3}\left(\frac{627}{32}\right) - \frac{67}{2} + \frac{\sqrt{2367483-1366816\sqrt{3}}}{32} = 0.731\cdots \tag{33}$$

This implies, $\nu_2 = 0.452\cdots$, which may be regarded as an estimate of the true exponent that would be obtained by direct numerical calculation on an enormous grid; see section 4. A similar analysis can be conducted for the DA(2, 6) model, we obtain $\Lambda = 4/5$ and $\nu_2 = 0.322\cdots$.

In the DA(3, 6) model, the results analogous to (2.24)–(2.26) are

$$T_{n+1} = \frac{T_n(w_n+3)^2(w_n+1)}{(5w_n-1)(4(3w_n-1)-T_n(w_n+1)(5w_n-1))} \tag{34a}$$

$$w_{n+1} = \frac{4T_n(w_n+1)(5w_n-1)(1-w_n)}{(w_n+3)^2} + 2\left(\frac{5w_n-1}{w_n+3}\right)^2 - 1 \tag{34b}$$

with $T_{n+1} = T_n = T^{*} = 0$, $w_{n+1} = w_n = w^{*}$, we obtain

$$(w^{*} - 1)(w^{*2} - 42w^{*} - 11) = 0 \tag{35}$$

hence

$$w^{*} = 1,\ 21 \pm 2\sqrt{113} \tag{36}$$

The stable fixed point is $w^{*} = 21+2\sqrt{113} = 42.26\cdots$. Following the same procedure as above, we obtain $\Lambda = 0.83\cdots$ and $\nu_2 = -\log(\Lambda)/\log(2) = 0.28\cdots$.

It is interesting to follow the evolution of the (T_n, R_n) point as we iterate equations (4) with (5) or (6) in $d = 2,3$ respectively; the corresponding physical picture is Figure 1*a* (for $d = 2$). This is illustrated in Figures 2*a* and 2*b* respectively, where in both cases, we see the different trajectories for various choices of (T_0, R_0) converging in the thick cloud limit, i.e., at $(T,R) = (0,1)$, but with different slopes. These initial choices are equivalent to various choices of DA phase function as described in the preceding subsection, and the convergence illustrates the fact that the scaling exponent $\nu_2(d)$ has no memory of this phase function, i.e., it is "universal" (in the sense of nonlinear dynamical systems). Other relevant results on direct transmittance in multifractal clouds, as well as total transmittance in plane parallel multifractal clouds can be found in Lovejoy et al 1990, Davis et al 1990.

3. Asymptotic Scaling Properties of a Fractal Cloud and the Effect of Boundary Conditions

3.1. *Fractals as Simple Inhomogeneous Scaling Systems*

The fractal clouds studied in this section can be viewed as straightforward generalizations of the internally homogeneous cloud models described and studied in the previous section. Rather than being homogeneous over a set with dimension equal to that in which the cloud is embedded, it is now "fractally homogeneous", i.e., homogeneous over a fractal set with dimension less than that of the embedding space. The main difference is that instead of modeling inhomogeneity at a very specific scale (essentially, the size of the cloud), we consider clouds in which inhomogeneities appear by construction at all scales (from the size of the unit cell to that of the complete cloud). We shall first consider the case of an isolated fractal cloud which can be analyzed following the same methods applied above to the internally homogeneous clouds; then we shall consider cyclic boundary conditions. This will allow us to independently assess the effects of finite horizontal extent and holes.

The cloud model discussed below is in fact a kind of deterministic two-dimensional "β model" for turbulence with an inner cutoff at some physical scale corresponding to an optical thickness τ_0 (see part 3 for more details). *Gabriel et al.* [1986] investigated numerically a random β model using DA(3, 6) radiative transfer on a (cubic) lattice and compared its (average) liquid water content with that of plane-parallel clouds of identical albedo; this yields systematically lower values for the latter. The following deterministic model explains this finding qualitatively; it is summarized in *Lovejoy et al.* [1989]. Interestingly enough, the random β model (although itself described by a single fractal dimension) exhibits multifractal DA radiation fields across the cloud top; this is not unlike the Earth's own cloud fields as measured by GOES radiometry in both VIS and IR channels [*Gabriel et al.*, 1988].

3.2. *A D=log3/log2 Cloud With Open Boundary Conditions*

In this section we apply the renormalization approach developed in section 2 to the simplest fractal cloud imaginable, shown in its early stages of construction in Figure 3, where the (internally uniform) purely scattering regions are shaded and the empty cells (clustering into huge holes) are white. Starting at a small inner scale with optical thickness τ_0 (below which the cloud has different, e.g., homogeneous behavior), we generate thicker and thicker clouds by placing three squares obtained at a previous iteration in the square pattern shown (this fourth square is empty). At each iteration, the mean optical depth increases by a factor 3/2; from the inner scale up to the resulting outer scale, the cloud is a scaling (monodimensional) fractal with dimension

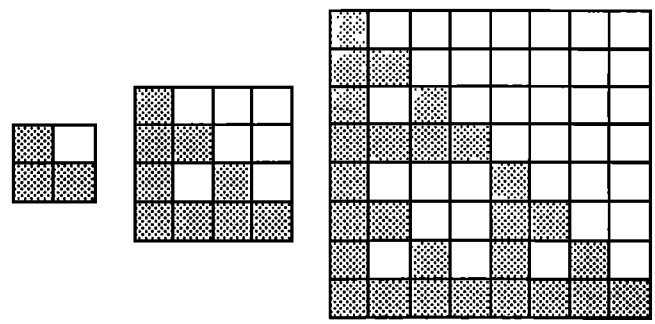

Fig. 3. Generator for the deterministic fractal medium embedded in $d = 2$ space with "dimension" $D = \log_2(3) = \log(3)/\log(2) = 1.58\cdots < d$; the first three stages in its construction are illustrated. Each iteration doubles the physical thickness but the total number of cells is only increased by a factor $3 = 2^D$ (this determines D, in analogy with the full square, where it is a factor $4 = 2^d$). It follows that the optical thickness (averaged across any side) is multiplied by $3/2 = 2^{1-C}$, where C is the fractal's "co-dimension" d-D, which is a direct measure of the sparseness of the medium.

$D = \log 3/\log 2 = 1.58\cdots$. Following exactly the same procedure as for the DA(2, 4) system used for investigating square clouds described in section 2, we can obtain approximate doubling relations for DA radiative transfer in fractal clouds (necessary modifications for the fractal are indicated in Appendix B). The corresponding doubled transmission and reflection coefficients for this fractal cloud are

$$T_{n+1} = \frac{T_n(1+T_n)}{2} + \frac{S_n^2}{2} + \frac{\Gamma_n^2}{2(1-R_n^2\Gamma_n^2)}\left\{R_n^2(1-R_n^2)(1+\frac{T_n^2}{S_n^2}) + T_n(1+2R_n+T_n^2R_n^2) + R_nS_n^2 + R_n^2S_n^2 + R_n(1-R_n^2)\right\}$$

$$R_{n+1} = R_n + \frac{\Gamma_n^2}{2(1-R_n^2\Gamma_n^2)}\left\{R_n(1-R_n^2)(1+\frac{T_n^2}{S_n^2}) + T_n(2+R_nT_n) + R_nS_n^2\right\} \quad (37)$$

where

$$\Gamma_n = \frac{S_n}{1-R_n^2} \quad (38)$$

and we have used the notation $T_n=T(\tau)$, $T_{n+1}=T(1.5\tau)$, $R_n=R(\tau)$, $R_{n+1}=R(1.5\tau)$, $S_n=S(\tau)$, $S_{n+1}=S(1.5\tau)$.

Conservative scattering can again be considered by requiring $R+T+2S = 1$; however questionable for such an asymmetrical fractal, the (implicit) assumption that both side losses are equal is consistent with the approximations used in Appendix B to obtain (37)–(38). We then obtain the basic physically significant fixed points (T^*,R^*) are (0,1), (1,0), corresponding to thick and thin clouds, respectively. We also have the following (nonphysical but real) fixed points (5,-5), (0.3416···,-0.4472···), (∞,-∞). As we iterate these equations we systematically build up the fractal cloud (as shown in Figure 3), and obtain a T–R plot showing successive iterations with different trajectories for various choices of (T_0, R_0); see Figure 2*c*.

Following the procedure outlined in subsection 2.4, we find that the thick cloud limit depends on the Jacobian of the nonlinear $(T_n,R_n)\rightarrow(T_{n+1},R_{n+1})$ mapping (**f**), which in turn depends on the direction at which the point (0,1) is approached; we again introduce the negative direction tangent $w = (1-R)/T$, and eliminate R. This results in a new map $(T_n,w_n)\rightarrow(T_{n+1},w_{n+1})$ which, in the neighborhood of $T = T^* = 0$ yields

$$w_{n+1} = \frac{(2w_n-1)(3w_n+1)(5w_n-1) - 2w_n(w_n-1)^2}{4w_n(w_n-1)^2 + (3w_n+1)(5w_n-1)} \quad (39)$$

Since we are interested in the behavior near the attracting fixed point $(T,R)\rightarrow(0,1)$, we seek solutions satisfying $w_{n+1} = w_n = w^*$. This yields $w^* = 1$ and

$$4w^{*3} - 13w^{*2} + 1 = 0 \quad (40)$$

whose roots are -0.2666, 0.2907, and 3.2260. A lengthy analysis of the new Jacobian near each of these four fixed points shows that the only attracting fixed point is $T^* = 0$, $w^* = 3.2260$. The thick cloud scaling exponent is now obtained from the largest eigenvalue (Λ) of the Jacobian (**J**) of **f** evaluated at the fixed point; see (31) which calls for its trace (Tr **J**) and its determinant (det **J**). Evaluating these, we obtain

$$\mathrm{Tr}\,\mathbf{J} = \frac{3}{2} - \frac{3(w^*-1)(1+2w^*)}{2(3w^*+1)(5w^*-1)} \quad (41)$$

$$\det \mathbf{J} = \frac{1}{2} + \frac{1}{4w^*} + \frac{(w^*-1)(1+2w^*)(1-10w^*)}{8w^*(3w^*+1)(5w^*-1)} \quad (42)$$

Each iteration corresponds to a doubling of the physical size and to an increase by a factor 3/2 of the average optical thickness. Denoting the doubling exponent of τ for this $D = 1.58\cdots$ cloud by $\nu_2(1.58)$ and inserting the value $w^* = 3.2260$ into eq. (3.6), we obtain $\Lambda = 0.942$ and hence:

$$\nu_2(1.58) = \frac{-\log(\Lambda)}{\log(3/2)} = 0.147$$

This exponent is an estimate of that which would be obtained by direct numerical calculation on an enormous grid with T≈0, R≈1 for each grid element.

3.3. *Periodic Boundary Conditions*

All of the models studied in the previous subsection feature light "leakage" through the sides, a feature which is not unrealistic in the case of sparse cloud fields, where very little reflected light from one cloud illuminates another. Conversely, in dense cloud fields, individual clouds cannot be considered isolated, and the radiation leaking out of the sides of one cloud would serve as inputs into the sides of neighboring clouds. As mentioned in the introduction of part 1, this dichotomy is artificial, and more realistic models should involve highly variable cloud fields which do not separate the two situations. At any rate, a well documented situation [see *Tsay and Jayaweera*, 1984] worth modeling is the extended cloud deck exhibiting internal inhomogeneity.

Fortunately, it is easy to make a renormalization estimate of this effect by imposing periodic boundary conditions in the horizontal, and studying the effect of the internal inhomogeneities alone (without side losses). The calculation proceeds in two steps. First, the same doubling geometry is used as before, and the system of linear equations this time appropriate for cyclic boundary conditions is set up, and solved for the total transmission and reflection. Since there is no leakage, the sum of the reflected and transmitted fluxes is 1 (ensuring that the corresponding exponents will be equal). The second step is to use the thick cloud formulas for the individual scattering elements, which means assuming the transmittance T is a small quantity, and $1-R = w^*T$ with $w^* = 3.2260$ (as above). With this thick element approximation (ignoring terms second and higher order in T), we obtain

$$D(\tfrac{3}{2}\tau) = 1 - U(\tfrac{3}{2}\tau) = \frac{(1+w^*)(2w^*+1)}{3+5w^*}T(\tau) \quad (44)$$

where $U(1.5\tau)$ is the total upwelling flux (cyclic boundary conditions albedo, $D = 1.58\cdots$) and $D(1.5\tau)$ its downwelling counterpart. Recall that R, T are the corresponding values in the noncyclic case. To obtain the (unique) cyclic exponent, we must now express $U(\tau)$, $D(\tau)$ in terms of $T(\tau)$, $R(\tau)$. Consider a single cell with unit incoming radiation along the top, with periodic boundary conditions in the horizontal. Denote the horizontal intensities by H, the left and right intensities must be equal when (spatially) averaged over an extended medium; applying the definitions of the transfer coefficients, we obtain $H = S + HT + HR$ (hence $H = 1/2$) as well as $U = R+2HS = R+S$ and $D = T+2HS = T+S$. Thus, to within our doubling approximation, we find

$$U(\tau) = R(\tau) + S(\tau)$$
$$D(\tau) = T(\tau) + S(\tau) \quad (45)$$

i.e., half the flux "recycled" by the periodic boundary conditions ($2S(\tau)$) is redirected up and the other half, down. Needless to say, this is a very rough approximation, but it is consistent with our previous assumptions of single-cell uniformity. In thick clouds, we have

$$S(\tau) = \frac{1}{2}[1-R(\tau)-T(\tau)] = \frac{w^*-1}{2}T(\tau) \quad (46)$$

Hence

$$D(\tau) = 1-U(\tau) = \frac{w^*+1}{2}T(\tau) \quad (47)$$

Thus, for the thick limit (and taking $w^* = 3.2260$),

$$\frac{D((3/2)\tau)}{D(\tau)} = 2\left(\frac{2w^*+1}{3+5w^*}\right) = 0.779 \quad (48)$$

Hence, $D(\tau) \approx \tau^{-\nu_{2cyc}(1.58)}$, where

$$\nu_{2cyc}(1.58) = -\frac{\log(0.779)}{\log(3/2)} = 0.616 \quad (49)$$

4. Accuracy of the Doubling Exponents

4.1. *Refinement of the Doubling Estimate: Quadrupling, Octupling, etc.*

As mentioned in the previous sections, the analytical estimates of ν_2 for various geometries only approximate the exponent that would be found by simulation on an enormous grid with each of the single-cell transfer coefficients having $R \approx 1$, $T \approx 0$. The transfer on such a grid can be better approximated by replacing "doubling" by "quadrupling", etc., which is best done numerically. First, (1) and (2) are solved on 2x2 through 16x16 arrays (by factors of 2) using the appropriate geometry. The outcome is then recycled as the new transfer coefficients in (2). In fact, *Gabriel* [1988] obtains computationally exact solutions in closed form for finite media discretized on orthogonal grids of any size in $d = 2,3$; in all other cases, over-relaxed iteration is used (see Appendix A, part 3). This procedure yields exponents ν_2 through ν_{16}, which approach the limiting value ν_{R^-}. The negative sign in the index underlines the fact that since $R \approx 1$, $T \approx 0$, these exponents correspond to $pq < 0$, and will not in general be the same as would be obtained with the physically significant phase functions with $pq > 0$.

Figures 4*a* and 4*b* show the results for squares in $d = 2$ indicating $\nu_{R^-}(2) = 3/4$ (c.f. the doubling estimate $\nu_2(2) = 0.45\cdots$), cubes in $d = 3$ yields $\nu_{R^-}(3) = 1/2$ (c.f. $\nu_2(3) = 0.28\cdots$). These exponents are written in the form of (small) whole number fractions, since they are obtained from numerical solutions of linear systems of partial differential equations with regular boundary conditions (see parts 1 or 3); hence we do not expect the appearance of irrational exponents. Figure 4*c* corresponds to the same refinement procedure applied to the $D = 1.58\cdots$ fractal cloud (with open boundary conditions); in this case, the exponent $\nu_{2^m}(1.58)$ is a slowly decreasing function of m, which indicates $\nu_{R^-}(1.58) \approx 0.16$ (c.f. $\nu_2(1.58) = 0.147$). For this kind of medium, there is no reason to argue for a ratio of small integers.

4.2. *Direct Numerical Simulation and Universality With Respect to Lattice Type*

Using numerical simulation, we can address the question whether the independence of the scaling exponents on DA phase

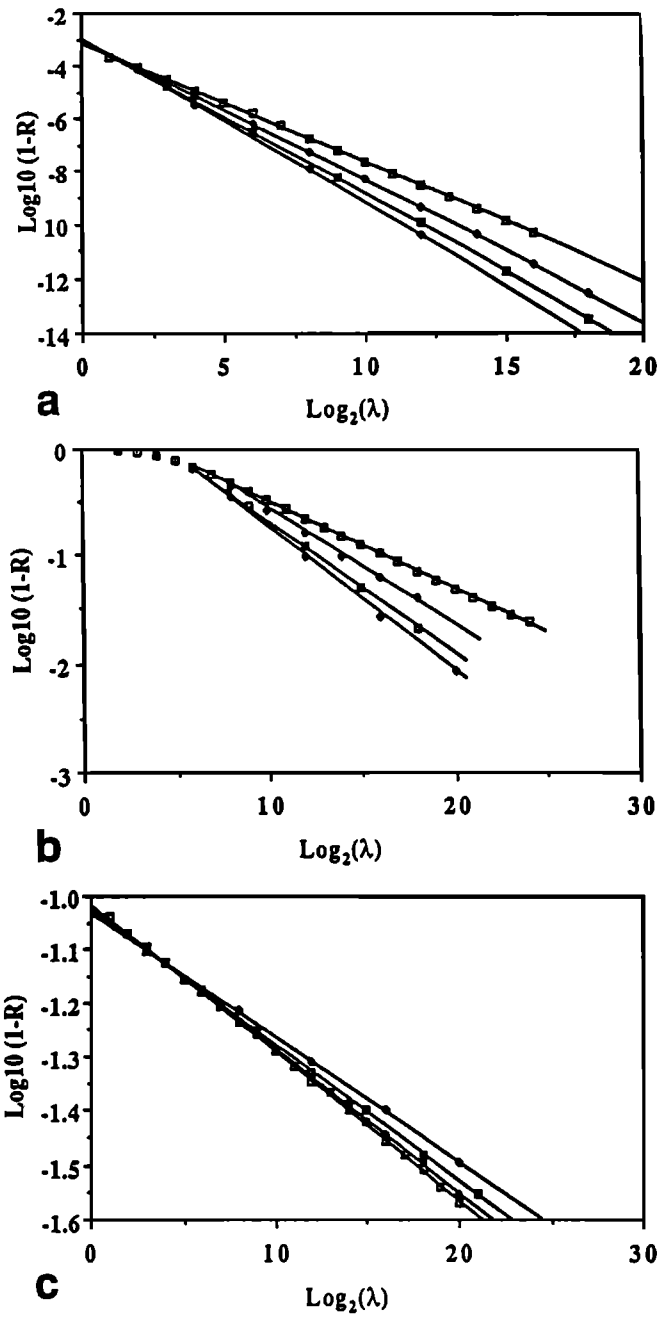

Fig. 4. Determination of the exponents $\nu_2, \nu_4, \nu_8, \nu_{16}$ for (*a*) $d = 2$ which determine the rate of convergence (left to right) toward the fixed point $R^* = 1$ and $T^* = 0$ for (top to bottom) doubling, quadrupling, octupling, and hexadecupling respectively. The λ is the physical size of the square in units of cell size, which is proportional to τ. The top line has the theoretically predicted (absolute) slope of $\nu_2 = 0.447\cdots$. The transfer coefficients for basic unit cells were $R = 0.9$, $T = 0.05$; hence $S = 0.025$, corresponding to a square of optical thickness $\tau_o \approx 100$ [see *Davis et al.*, 1989]. The slopes are seen to be accumulating toward 0.75, corresponding to a ratio of small integers for $\nu_{R^-} = 3/4$. (*b*) For $d = 3$ we find $\nu_{R^-} = 1/2$ with $\nu_2 = 0.28\cdots$; it was initiated with cubic cells described by $R = 0.5625$, $T = 0.0089$, $S = 0.10715$ (these were obtained by *Davies* [1976] from a Monte Carlo simulation for a cube of optical thickness $\tau_o = 100$, illuminated normally with a Deirmendjian C1 drop size distribution at 0.45 μm wavelength, $g \approx 0.85$). (*c*) For the $D = 1.58\cdots$ fractal in $d = 2$, where λ is proportional to $\tau^{1/(1-C)}$ with $C = d-D = 0.42\cdots$, the same single (square) cell transfer coefficients were used initially and the procedure yields $\nu_{R^-} \approx 0.16$ with the renormalization estimate $\nu_2 = 0.147$ now on the bottom. In order to obtain ν_{2^m} ($m = 1,2,3,4$) the slopes on the graph must be divided by $(1-C)\log_{10}(2)$ in all cases.

functions can be extended to different angular discretizations, which are really just other DA phase functions. An obvious way to test this hypothesis is to estimate ν_{R^-} using the triangular lattice configuration in $d = 2$ discussed in section 2 (and Appendix D for further details). We therefore solved the triangular lattice DA equations (D1) numerically, obtaining results which are virtually identical to the square results, $\nu_{triangle} = \nu_{square} = \nu_{R^-} = 3/4$. This supports the conjecture that the universality of ν_{R^-} holds independent of lattice type, equivalently (here), angular discretization. Direct calculations give not only ν_{R^-} but also ν_{T^-} ($\nu_{T^-} = \nu_{R^-}$ only for boundary conditions where the sides do not act as sinks for radiation); in both square and cubic clouds, we find $\nu_{T^-} = 1$, i.e. the (d=1) value predicted in Part I for internally homogeneous media in any dimension which we expect to be dominated by diffusion.

Direct numerical solutions were also obtained for 2x2 through 16x16 grids for the $D = 1.58\cdots$ fractal cloud; we find $\nu_{R^-}(1.58) \approx 0.162$, which is quite close to the doubling value $\nu_2(1.58,\text{open}) = 0.147$. The corresponding transmission exponent is $\nu_{T^-}(1.58,\text{open}) \approx 0.69$. In the case of periodic boundary conditions, direct numerical solutions yield $\nu_{R^-}(1.58,\text{cyclic}) = \nu_{T^-}(1.58,\text{cyclic}) \approx 0.60$, which is again fairly close to the corresponding doubling estimate $\nu_2(1.58,\text{cyclic})=0.616$.

To understand why $\nu_{T^-} > \nu_{R^-}$, recall that $w = (1-R)/T \approx \tau^{\nu_{T^-}-\nu_{R^-}} = 1+2(d-1)S/T$; since T must approach zero faster than S as τ increases indefinitely we obtain $\nu_{T^-} > \nu_{R^-}$. Notice that all the cases studied verify the double inequality $1 \geq \nu_{T^-} \geq \nu_{R^-}$ with the former equality applying for internally homogeneous systems and the latter for periodic systems (where $1-R = T$ in the above).

4.3. *The Fundamental Limitation of Renormalization in DA Radiative Transfer*

Although we have seen that doubling is not exact because of the approximation that for each iteration the intensity field is constant over half the size of the system, we might have expected (as is often the case) that quadrupling, octupling, etc., would lead to a converging series of improved approximations. Above, we saw that this was indeed the case, except that the improved approximations were with respect to the DA exponents characterized by the unphysical $pq<0$. In other words, the basic limitation of real space renormalization in DA radiative transfer is that more than one universality class exists (with generally different exponents), and the method gives the wrong one.

Let us consider the renormalization process in a bit more detail; in the remainder of this subsection, we refer to equations in part 1. Starting with (7), and considering thin clouds ($T \approx 1$), the eigenvalues of σ^2 are all ≈ 1, the gradients across each cell are small, and the doubling procedure gives an accurate estimate of the DA radiative transfer properties of the system (i.e., it reproduces the linear regime). As the iteration proceeds, T and R take on intermediate values; the gradients and the high order terms in the expansion (9) are no longer negligible. The reflection and transmission coefficients estimated by the doubling method are therefore in error by quantities depending on the magnitude of these terms. Eventually, when $R \approx 1$, $T \approx 0$, the eigenvalues of σ^2 are once again near 1, the fields are smooth and high order terms are negligible. The fields are thus solution of the (spatially continuous) DA radiative transfer equation (6); however, as indicated elsewhere (section 3 and Appendix A of Part I), with a negative phase function (matrix) **P**. Unfortunately, in spite of the decrease in importance of the high-order terms, unlike the thin cloud limit, the thick limit depends on the direction in (T,R) space from which the point (0,1) is approached (it depends on w), and the limiting value (w^*) will not be accurate.

Finally, we may ask whether the exponents obtained by numerically solving (7) with $R \approx 1$, $T \approx 0$ (which, as indicated, corresponds to solving (6) with unphysical, negative phase functions) are the same as those that would have been obtained on enormous grids with $T \approx 1$, $R \approx 0$ (or equivalently, DA Monte Carlo methods). In other words, are the universality classes (exponents) of (6) the same for positive and negative pq? Although we consider this question numerically in some detail in part 3, we can anticipate the results: the only case studied in which the exponents form $pq < 0$, $pq > 0$ are the same is in the DA(2,4) system for an internally homogeneous medium. Here, the identity of the exponents can be understood, since considering (45) we expect the $\delta_y^2\delta_x^2$ term to dominate near the top of the cloud, where the light comes in, imposing a large gradient in intensity, and hence to determine ν_R, while the $(\delta_y^2+\delta_x^2)$ diffusion term dominates the bulk of the system, far from the top boundary, and hence determines ν_T. It is only in this homogeneous two-dimensional case, that the relative sign between the two terms, i.e., sign(pq), is unimportant in determining the exponents.

5. Conclusions

We have presented an approach called "real space renormalization", which we use for studying discrete angle radiative transfer in scaling systems, and which is really just a generalization of invariant imbedding methods to scaling systems of which the plane-parallel kind are only the simplest examples. The method works by starting with transfer coefficients for optically thin clouds and estimating the corresponding coefficients in thicker clouds obtained by doubling (or more generally, quadrupling, octupling, etc.). One obtains a nonlinear mapping which transforms the coefficients at one scale to a larger (e.g., doubled scale). The thick and thin cloud behavior is then obtained as a power law approach to fixed points of the mapping with exponents universal, in the sense that they are independent of the phase function.

Although the method correctly reproduces the basic features of radiative transfer in these scaling systems, including both the phase function sensitivity for thin clouds, and insensitivity (universality) for the thick clouds, as well as the scaling behavior of the transmission and albedo, the quantitative predictions are poor primarily because two main universality classes exist, and the method converges to the unphysical one.

Appendix A: DA(1, 2) Radiative Transfer System for Conservatively Scattering Layered Media

It is interesting to see that the simple DA(1, 2) system (which was shown in part 1 to be equivalent to the two-flux approximation of continuous angle radiative transfer) can be solved without recourse to calculus for the solution of a two-point boundary value problem. This alternative approach makes use of the "adding" of two finite layers and provides a good example of the power of invariant imbedding techniques.

Let layer the first layer ($R(\tau_1)$,$T(\tau_1)$) lay between (optical) coordinates 0 and τ_1, and the second layer ($R(\tau_2)$,$T(\tau_2)$) extends beyond, between τ_1 and $\tau = \tau_1+\tau_2$; the ordering corresponds to light propagation. The interaction principle [*Preisendorfer*, 1965] expressed in (1), with definitions (2) in mind, yields

$$\begin{aligned} I_+(\tau_1) &= T(\tau_1)I_+(0)+R(\tau_2)I_-(\tau_1) \\ I_+(\tau) &= T(\tau_2)I_+(\tau_1)+R(\tau_2)I_-(\tau) \\ I_-(0) &= T(\tau_1)I_-(\tau_1)+R(\tau_1)I_+(0) \\ I_-(\tau_1) &= T(\tau_2)I_-(\tau)+R(\tau_1)I_+(\tau_1) \end{aligned} \qquad \text{(A1)}$$

Boundary conditions are $I_{-}(0)=1$, $I_{+}(\tau)=0$ and, by definition, $I_{+}(0)=R(\tau)$, $I_{-}(\tau)=T(\tau)$. Eliminating the intensities, we obtain the following nonlinear relationship between the various σ coefficients:

$$R(\tau_1+\tau_2) = R(\tau_1) + \frac{R(\tau_2)T(\tau_1)^2}{1-R(\tau_1)R(\tau_2)} \qquad (A2a)$$

$$T(\tau_1+\tau_2) = \frac{T(\tau_1)T(\tau_2)}{1-R(\tau_1)R(\tau_2)} \qquad (A2b)$$

These relations have an interesting physical interpretation: expanding the (common) denominator in a Taylor series, we see that each term corresponds to a specific number of (diffuse) reflections between the two layers. This natural approach to radiative transfer has been used in model building; for instance, *Tanré et al.* [1979] use (A2*a*) with $R(\tau_2)$ identified as a ground reflectance. The functional equations (A2*a*) and (A2*b*) can be solved exactly, the simplest case being non-absorbing systems where we can use radiant energy conservation ($T+R = 1$) to eliminate the reflectancies. We are left with

$$T(\tau_1+\tau_2) = \frac{T(\tau_1)T(\tau_2)}{T(\tau_1)+T(\tau_2)-T(\tau_1)T(\tau_2)} \qquad (A3)$$

or, after rearrangement

$$\frac{1}{T(\tau_1+\tau_2)} - 1 = \frac{1}{T(\tau_1)} - 1 + \frac{1}{T(\tau_2)} - 1 \qquad (A4)$$

The general solution of the functional equation (A4) is thus

$$\frac{1}{T(\tau)} - 1 = C\tau \qquad (A5)$$

hence

$$T(\tau) = \frac{1}{1+C\tau} \qquad (A6)$$

The arbitrary constant C can be determined by considering the thin cloud limit ($\tau\to 0$) where we have $T \approx 1-C\tau$ and identifying with the single-scattering approximation. This yields $C = 1-t = r = (1-g)/2$ thus retrieving (B6*a*) of part 1 using the notations of section 2.3 above or section 3.3 of part 1.

Appendix B: Details on Doubling in the Square and Fractal Clouds

B.1. *The Homogeneous Square Cloud*

We illustrate this method in detail within DA(2, 4) radiative transfer by calculating the coefficients of the 2x2 square made up of square cells with $S(\tau)$, $T(\tau)$, $R(\tau)$ coefficients, as shown in Figure 1*a* (where we take the origin to be in the lower left corner). We now irradiate the square with unit radiation incident on the top face only (i.e. the boundary conditions are $I_{-y}(x,2\tau) = 1$, $I_{+y}(x,0) = 0$ for $0\le x\le 2\tau$, and $I_{-x}(2\tau,y) = I_{+x}(0,y) = 0$ for $0\le y\le 2\tau$). We obtain

$$R(2\tau) = \left\{ \int_0^{\tau} I_{+y}(x,2\tau)dx + \int_{\tau}^{2\tau} I_{+y}(x,2\tau)dx \right\} \Big/ \left\{ \int_0^{2\tau} I_{-y}(x,2\tau)dx \right\}$$

$$= \frac{1}{2\tau}\left\{ \int_0^{\tau} I_{+y}(x,2\tau)dx + \int_{\tau}^{2\tau} I_{+y}(x,2\tau)dx \right\} \qquad (B1)$$

Similarly,

$$T(2\tau) = \frac{1}{2\tau}\left\{ \int_0^{\tau} I_{-y}(x,2\tau)dx + \int_{\tau}^{2\tau} I_{-y}(x,2\tau)dx \right\} \qquad (B2)$$

$$S(2\tau) = \frac{1}{2\tau}\left\{ \int_0^{\tau} I_{-x}(0,y)dy + \int_{\tau}^{2\tau} I_{-x}(0,y)dy \right\} \qquad (B3)$$

We have split up the limits of integration in this way, since it suggests a simple approximate method for estimating the doubled reflectivity, transmissivity, and side-scattering coefficients ($R(2\tau)$, $T(2\tau)$, $S(2\tau)$) by replacing the intensity function over each face by a constant function equal to the average. This is the crucial approximation, a kind of "mean field" assumption. Using the notation

$$I_{\pm y}(n,m) = \frac{1}{2\tau}\left\{ \int_{m\tau}^{(n+1)\tau} I_{\pm y}(x,m\tau)dx \right\} \qquad (B4)$$

$$I_{\pm x}(n,m) = \frac{1}{2\tau}\left\{ \int_{m\tau}^{(m+1)\tau} I_{\pm x}(n\tau,y)dy \right\}$$

with m and n the integers 0, 1, 2. We obtain the following expressions for the coefficients from (B1)–(B4):

$$\begin{aligned} R(2\tau) &= \tfrac{1}{2}\left(I_{+y}(0,2) + I_{+y}(1,2)\right) \\ T(2\tau) &= \tfrac{1}{2}\left(I_{-y}(0,0) + I_{-y}(1,0)\right) \\ S(2\tau) &= \tfrac{1}{2}\left(I_{+x}(2,0) + I_{+x}(2,1)\right) = \tfrac{1}{2}\left(I_{-x}(0,0) + I_{-x}(0,1)\right) \end{aligned} \qquad (B5)$$

If we now maintain this uniformity approximation for all the radiation fields inside the square, then each τ x τ square can be regarded as a unit cell, and we can then apply (1) to estimate the $I_i(n,m)$. Since there are 12 boundaries with fluxes crossing each in two directions, there are 12 x 2 = 24 simultaneous (linear) equations to be solved for the various $I_i(n,m)$ values (note that for many of the values of m,n, the equations for the components $I_i(n,m)$ are trivial, and are not included in the above). Since there is also left/right symmetry, this is reduced to only 12. Using the boundary conditions

$$\begin{aligned} I_{-y}(0,2) &= 1 & I_{-y}(1,2) &= 1 \\ I_{+y}(0,0) &= 0 & I_{+y}(1,0) &= 0 \\ I_{-x}(2,1) &= 0 & I_{-x}(2,0) &= 0 \\ I_{+x}(0,0) &= 0 & I_{+x}(0,1) &= 0 \end{aligned} \qquad (B6)$$

the system of equations describing the intensity emerging at the boundaries is, from (1) and (2),

$$\begin{aligned} I_{+y}(0,2) &= R+SI_{-x}(1,1) + TI_{+y}(0,1) \\ I_{-y}(0,0) &= TI_{-y}(0,1) + SI_{-x}(1,0) \\ I_{-x}(0,1) &= SI_{-y}(0,2) + SI_{+y}(0,1) + TI_{-x}(1,1) \\ I_{-x}(0,0) &= SI_{-y}(0,1) + TI_{-x}(1,0) \end{aligned} \qquad (B7)$$

whereas the remaining internal fields are found from

$$\begin{aligned} I_{-x}(1,1) &= S+RI_{+x}(1,1) + SI_{+y}(1,1) \\ I_{-y}(0,1) &= T+SI_{-x}(1,1) + RI_{+y}(0,1) \\ I_{+y}(0,1) &= RI_{-y}(0,1) + SI_{-x}(1,0) \\ I_{+x}(1,0) &= SI_{-y}(0,1) + RI_{-x}(1,0) \end{aligned} \qquad (B8)$$

Finally, by left/right symmetry

$$I_{\pm y}(0,m) = I_{\pm y}(1,m) \qquad m = 0,1,2$$
$$I_{\pm x}(1,m) = I_{+x}(1,m) \qquad m = 0,1 \tag{B9}$$

This yields an additional 10 equations, of which two are the same as (B6), yielding a total of 24 equations for 24 unknowns. Solving (B6) to (B9) for $I_{+y}(0,2)$, $I_{+y}(1,2)$, $I_{-y}(0,0)$, $I_{-y}(1,0)$, $I_{+x}(2,0)$, and $I_{+x}(2,1)$ and substituting into (B5), we obtain (4) for $d = 2$ and (5).

B.2. *Modifications for the 1.58-D Fractal Cloud*

Equations (37) and (38) are derived by solving the 24 linear equations of subsection B.1 with the boundary conditions modified to correspond to the 2X2 square with an upper (right) corner hole as shown in Figure 3. The left/right symmetry invoked no longer holds, and the eight equations replacing (B9) are, from (1) and (2) as well as boundary conditions

$$\begin{aligned} I_{-x}(1,1) &= 0 \\ I_{-y}(1,1) &= 1 \\ I_{+y}(1,2) &= I_{+y}(1,1) \\ I_{+x}(2,1) &= I_{+x}(1,1) \\ I_{+y}(1,1) &= RI_{-y}(1,1) + SI_{+x}(1,0) \\ I_{-x}(1,0) &= SI_{-y}(1,1) + RI_{+x}(1,0) \\ I_{-y}(1,0) &= TI_{-y}(1,1) + SI_{+x}(1,0) \\ I_{+x}(2,0) &= TI_{+x}(1,0) + SI_{-y}(1,1) \end{aligned} \tag{B10}$$

If cyclical boundary conditions were applied, the (external) boundary conditions (B6) must be modified to read

$$\begin{aligned} I_{-y}(0,2) &= 1 & I_{-y}(1,2) &= 1 \\ I_{+y}(0,0) &= 0 & I_{+y}(1,0) &= 0 \\ I_{-x}(2,1) &= I_{-x}(0,1) & I_{-x}(2,0) &= I_{-x}(0,0) \\ I_{+x}(0,0) &= I_{+x}(2,0) & I_{+x}(0,1) &= I_{+x}(2,1) \end{aligned} \tag{B11}$$

APPENDIX C: RENORMALIZATION IN THE CASE OF NONCONSERVATIVE SCATTERING

We have seen, by expanding the doubling function near fixed points in Taylor series, that (local) scaling (rather than exponential) behavior is generally obtained. This derivation is so general that at first sight it would appear to apply not only to conservative scattering, but also to nonconservative scattering. This is the converse of the usual arguments which yield exponential type behavior for thick absorbing clouds, with algebraic behavior only as a special case (when the absorption is exactly zero); see, for example, for the DA(1, 2) model detailed in Appendix B of part 1. In this appendix, we show how this apparent contradiction is resolved by the fact that the nonconservative cases involve degenerate Jacobians.

Let f be the two-dimension nonlinear map $(R,T)_n \rightarrow (R,T)_{n+1}$. We have seen that in the conservative scattering cases examined, the Jacobian matrix evaluated at the thick cloud fixed point $(\partial f(R,T)/\partial(R,T)|_{T^*,R^*})$ is nondegenerate (it has a nonzero determinant). Below, we show that all first-order derivatives are zero (with the exception of $\partial R_{n+1}/\partial R_n|_{T^*,R^*} = 1$), and hence $[\partial f(R,T)/\partial(R,T)|_{T^*,R^*}]^n$ is no longer approximated by Λ^n (recall that Λ is the largest eigenvalue). To see how this leads to exponential behavior, we study the simple DA(1, 2) case with absorption, although it is not hard to see that the results will hold in the other models studied. The relevant doubling mapping can be obtained from (4) by putting $S = \Gamma_1 = 0$:

$$\begin{aligned} T_{n+1} &= \frac{T_n^2}{1 - R_n^2} \\ R_{n+1} &= R_n(1 + T_{n+1}) \end{aligned} \tag{C1}$$

Writing the thick cloud fixed point as $(0,R^*)$, and expanding to second order, we obtain

$$\Delta T_{n+1} = \frac{\Delta T_n^2}{1 - R^{*2}} \tag{C2a}$$

$$\Delta R_{n+1} = \Delta R_n + R^* \Delta T_{n+1} \tag{C2b}$$

The solution to these equations is obtained by taking $y_n = \log \Delta T_n$, and solving the resulting linear finite difference equation for y_n. Recalling that $\tau_n = 2^n \tau_0$ and $T^* = 0$, hence $T_n = \Delta T_n$, we obtain:

$$T_n = \frac{1}{1 - R^{*2}} e^{-k_0 \tau_n} \tag{C3a}$$

$$k_0 = -\frac{\log \Delta T_0}{\tau_0} \tag{C3b}$$

which is an exponential transmission law (k_0 is positive) as expected. The expression for ΔR_n can now be obtained by inserting (C3) into (C2b) and performing finite integration; this would naturally yield $R^* < 1$. Similar results may be obtained for $d = 2,3$, although the algebra is much more involved. When the absorption is very small, but finite, we expect exponential behavior to arise only for extremely thick clouds, scaling (algebraic) regimes (with the previously determined exponents) should still hold, although now only over a finite range of optical thickness.

APPENDIX D: SPATIALLY DISCRETIZED EQUATIONS OF DA RADIATIVE TRANSFER ON A TRIANGULAR LATTICE

A slightly more complex situation arises than that described in the introduction (section 1) when the lattice cells do not all share the same orientation, such as in the case of the plane covered by equilateral triangles. In this case, upward pointing triangles (at lattice positions $\boldsymbol{m}$) have nonzero intensities only along directions $\pi/3$, π, $5\pi/3$ ($\boldsymbol{k}_1$, $\boldsymbol{k}_2$, $\boldsymbol{k}_3$, respectively, which are the vectors connecting the centers of upward pointing triangles with the surrounding downward pointing triangles); angles being measured from zenith. In comparison, downward pointing triangles (at positions $\boldsymbol{m}'$, where the $\boldsymbol{m}'$ vectors are displaced by $\boldsymbol{k}$ with respect to the lattice of upward triangles) have nonzero intensities along directions $4\pi/3$, 0, $2\pi/3$ (respectively, vectors $\boldsymbol{k}_1' = -\boldsymbol{k}_1$, $\boldsymbol{k}_2' = -\boldsymbol{k}_2$, $\boldsymbol{k}_3' = -\boldsymbol{k}_3$, connecting the centers of downward pointing triangles with the surrounding upward pointing ones). We therefore obtain from (1)

$$\begin{aligned} I_i(m) &= \sum_{k=k_1,k_2,k_3} \sigma_{ik}(m)\, I_k(m-k) \\ I_{-i}(m') &= \sum_{k'=k'_1,k'_2,k'_3} \sigma_{ik'}(m')\, I_{k'}(m'-k') \end{aligned} \tag{D1}$$

where σ_{ik} is a 3x3 matrix, the simplest of which is

$$\sigma = \begin{pmatrix} R & S & S \\ S & R & S \\ S & S & R \end{pmatrix} \quad \text{(D2)}$$

In section 2 we consider this DA(2, 6) system analytically, and it is exploited numerically in section 4. Note that since the eigenvalues of the above matrix are R-S, R-S, 1-A, the latter will be nearly one when $A = 1\text{-}R\text{-}2S \approx 0$, $R \approx 1$ yielding smooth intensity fields and good numerical approximations to the corresponding DA radiative transfer equation (but not necessarily with positively-valued phase functions!).

Acknowledgments. We wish to thank R. Davies, H. Leighton, N. Sakellariou, A. Saucier, G. Stephens, T. Warn, A. Royer, N. O'Niell and our anonymous referees for many helpful discussions and comments.

REFERENCES

Ambarzumian, V.A., Diffusion of light by planetary atmospheres, *Astron. Zh.*, *19*, p. 30, 1942.

Bell T.L., U. Frisch, and H. Frisch, Renormalization-group approach to noncoherent radiative transfer, *Phys. Rev.*, *A17*, 1049–1057, 1978.

Bellman R., R. Kalaba, and G.M. Wing, Invariant imbedding and mathematical physics, I, particle physics, *J. Math. Phys.*, *1*, 280–308, 1960.

Chandrasekhar, S., *Radiative Transfer*. Oxford University Press, New York, 1950. (Reprinted by Dover, New York, 1960.)

Cogley, A.C., Initial results for multidimensional radiative transfer by the adding/doubling method, paper presented at the 4th Conference on Atmospheric Radiation, Am. Meteorol. Soc., Toronto, June 12–16, 1981.

Davies, R., The three dimensional transfer of solar radiation in clouds, Ph.D. thesis, 219 pp, Univ. of Wisc., Madison, 1976.

Davis, A., P. Gabriel, S. Lovejoy, and D. Schertzer, Asymptotic laws for thick clouds, dimensional dependence - phase function independence, in *IRS'88: Current Problems in Atmospheric Radiation*, edited by J. Lenoble and J. F. Geleyn, pp. 103–106, A. Deepak, Hampton, Va., 1989.

Davis, A., P. Gabriel, S. Lovejoy, D. Schertzer, and G.L. Austin, Discrete angle radiative transfer, part 3, Numerical results and applications, *J. Geophys. Res.*, this issue.

Davis, A., Lovejoy, S., and D., Schertzer, Radiative transfer in multifractal clouds, in *Scaling, Fractals and Non-Linear Variability in Geophysics*, edited by D. Schertzer, and S. Lovejoy, Kluwer, Holland, in press, 1990.

Gabriel, P., S. Lovejoy, G.L. Austin, and D. Schertzer, Radiative transfer in extremely variable fractal clouds, paper presented at the 6th Conference on Atmospheric Radiation, Am. Meteorol. Soc., Williamsburg, Va., May 12–16, 1986.

Gabriel, P., Discrete angle radiative transfer in uniform and extremely variable clouds, Ph.D. thesis, 160 pp, Phys. Dep., McGill Univ., Montréal, Québec, 1988.

Gabriel P., S. Lovejoy, D. Schertzer, and G.L. Austin, Multifractal analysis of resolution dependence in satellite imagery, *Geoph. Res. Lett.*, *15*, 1373–76, 1988.

Hansen, J.E., Radiative transfer by doubling very thin layers, *Astrophys. J.*, *155*, 565–573, 1969.

Lovejoy, S., P. Gabriel, D. Schertzer, and G.L. Austin, Fractal clouds with discrete angle radiative transfer, in *IRS'88: Current Problems in Atmospheric Radiation*, edited by J. Lenoble and J. F. Geleyn, pp. 99–102, A. Deepak, Hampton, Va., 1989.

Lovejoy, S., A. Davis, P. Gabriel, G.L. Austin, and D. Schertzer, Discrete angle radiative transfer, part 1, Scaling and similarity, universality and diffusion, *J. Geophys. Res.*, this issue.

Lovejoy, S., A. Davis, D. Schertzer, Radiative transfer in multifractal clouds: observations and theory, paper presented at the 7th Conference on Atmospheric Radiation, Am. Meteorol. Soc., San Francisco, July 22-25, 1990.

Schuster, H.G., *Deterministic Chaos – An Introduction*, 2nd revised edition, XXIII+270 pp., VCH, Wienhiem, Germany, 1989.

Stephens, G.L., Radiative transfer in spatially heterogeneous, two-dimensional anisotropically scattering media, *J. Quant. Spectrosc. Radiat. Transfer*, *36*, 51–67, 1986.

Tanré, D., M. Herman, P.Y. Deschamps, and A. de Leffe, Atmospheric modeling for space measurements of ground reflectances, including bi-directional properties. *Appl. Opt.*, *18*, 3587–3594, 1979.

Tsay, S., and K. Jayaweera, Characteristics of arctic stratus clouds, *J. Climate Appl. Meteor.*, *23*, 584–596, 1984.

G. L. Austin and S. Lovejoy, Physics Department, McGill University, 3600 University Street, Montréal, Québec H3A-2T8. Canada.

A. Davis, D. Schertzer, Météorologie Nationale, EERM/CRMD, 2 Ave. Rapp, 75007 Paris, France.

P. Gabriel, CIRA, Dept. of Atmospheric Science, Colorado State University, Fort Collins, CO 80523.

(Received August 16, 1988;
revised May 17, 1989;
accepted September 19 1989.)